Research Article | Vol. 33, No. 9 / 5 May 2025 / Optics Express 19158

Optics EXPRESS

Low threshold InAs/InP quantum dot lasers

Jae-Seong Park,[1,*,†] Hui Jia,[1,4,†] Haotian Zeng,[1] Yangqian Wang,[1] Jiajing Yuan,[1] Jun Li,[1] Shangfeng Liu,[2] Calum Dear,[1] Kongming Liu,[1] Chong Chen,[1] Huiwen Deng,[1] Mickael Martin,[3] Qiang Li,[2] Thierry Baron,[3] Mingchu Tang,[1] Alwyn Seeds,[1] and Huiyun Liu[1]

[1] *Department of Electronic and Electrical Engineering, University College London, London WC1E 7JE, UK*
[2] *School of Physics and Astronomy, Cardiff University, Cardiff CF24 3AA, UK*
[3] *University Grenoble Alpes, CNRS, CEA/LETI-Minatec, Grenoble, LTM, Grenoble F-38054, France*
[4] *hui.jia@ucl.ac.uk*
[†] These authors contributed equally.
[*] *jae-seong.park@ucl.ac.uk*

Abstract: InAs/InP quantum dot (QD) lasers are promising light sources for optical communication due to their discrete energy states, offering advantages such as low threshold current density and enhanced thermal stability. However, challenges remain in achieving uniform QDs on the InAs/InAlGaAs/InP material system to ensure low threshold current density and high-temperature operation. This work demonstrates low threshold, high-temperature L-band InAs/InAlGaAs/InP QD lasers grown on InP (001) substrates with the indium-flush technique to optimize QD uniformity. The as-cleaved seven-stack QD lasers under pulsed injection exhibit a very low threshold current density of 69 A/cm^2 per QD layer and achieve a high maximum operating temperature of 130 °C. These results represent significant progress in InAs/InP QD laser development, highlighting the potential for high-performance semiconductor light sources in optical communication.

1. Introduction

The development of high-performance and reliable C-/L-band semiconductor lasers as light sources is of critical importance for optical communication systems due to the ever-growing data traffic demand, which has been further accelerated by recent advancements in artificial intelligence and machine learning applications [1–4]. Self-assembled InAs quantum dot (QD) lasers have been regarded as promising light sources because of various advantages enabled by their atom-like discrete energy states [5,6]. The delta function-like density of states of QDs offers key benefits over conventional quantum well (QW) lasers, including low threshold current density (J_{th}), temperature-insensitive operation, tolerance to optical feedback, and ultra-fast gain recovery [7–9]. As a result, substantial advances have recently been made in O-band InAs/GaAs QD lasers, including even the heteroepitaxial growth of QD lasers on silicon (Si) for monolithic integration into Si-based photonic integrated circuits [10–13].

In the case of C-/L-band InAs/InP QD lasers—key components for high-speed and long-haul optical communication, as well as eye-safe optical sensing—considerable advancements have also been achieved [14–16]. Various studies have demonstrated their potential for applications such as distributed feedback lasers, high-speed lasers, mode-locked lasers, *etc.* [17–21] However, compared to O-band InAs/GaAs QD lasers, progress in InAs/InP QD lasers has been relatively limited, particularly in terms of J_{th} and temperature-insensitive operation. This is primarily due to the lower lattice mismatch of ~3.2% in the InAs/InP material system, compared to ~7.2% in

#561471 https://doi.org/10.1364/OE.561471
Journal © 2025 Received 7 Mar 2025; revised 10 Apr 2025; accepted 10 Apr 2025; published 23 Apr 2025

the InAs/GaAs, which results in weaker strain energy for QD formation via Stranski-Kranstanov growth. Consequently, InAs/InP QDs exhibit a broader size distribution, necessitating stringent growth optimization to achieve uniform QDs [22]. These QDs suffer from insufficient gain, high J_{th}, and limited high-temperature operation. Moreover, elongated nanostructures, also known as quantum dashes, readily form along with the $[1\bar{1}0]$ direction due to the surface diffusion anisotropy of indium adatoms on the commonly used (001) InP substrate [23]. Therefore, to realize highly reliable C-/L-band QD lasers, it is of paramount importance to obtain high-quality, uniform QDs to ensure sufficient gain, low J_{th}, and enhanced thermal stability.

To address these challenges, a variety of approaches have been explored to improve the structural and optical properties of InAs QDs on InP, such as As-P exchange, strain engineering, tunnel injection QW structure, *etc*. [24–28] One promising strategy is the indium-flush technique, which uses separate first and second capping layers instead of a typical single capping layer after QD formation. This method promotes indium migration after the first capping layer by annealing, allowing precise control over the height of QDs. For example, Yuan *et al*. [29] recently demonstrated that applying the indium flush technique to InAs/InAlGaAs/InP QDs led to more uniform QD height, narrowing the full-width at half-maximum (FWHM) of room-temperature (RT) photoluminescence (PL) spectra from 89.2 to 47.9 meV, and reported a J_{th} per QD layer of 106 A/cm^2 in seven-stack InAs/InP QD lasers with a 50×1000 μm^2 cavity. Additionally, Wang *et al*. [30] reported a narrow PL FWHM of 40.1 meV in five-stack InAs/InAlGaAs/InP QDs employing the indium-flush technique and achieved a low J_{th} per QD layer of 80 A/cm^2 from 50×1000 μm^2 devices with a 97% high-reflection (HR) facet coating. Despite these advancements, further improvements are still required to achieve lower J_{th} and high-temperature operation to meet the demands of practical applications.

In this study, we demonstrate low-threshold L-band InAs/InAlGaAs/InP QD lasers grown on InP (001) substrates, capable of high-temperature operation. To obtain uniform height and emission wavelength of QDs in the InAs/InAlGaAs/InP material system, the indium-flush technique was applied. The as-cleaved seven-stack InAs/InP QD lasers exhibited a maximum operating temperature of 130 °C. The J_{th} at RT was measured to be 483 A/cm^2 under pulsed injection, corresponding to the J_{th} per QD layer of 69 A/cm^2. To the best of our knowledge, the J_{th} per QD layer of 69 A/cm^2 is the lowest value obtained in C-/L-band QD lasers on (001) InP.

2. Experiment

We began the growth of the InAs/InP QD laser structure on an n-type (001) InP substrate using the Veeco GEN 930 molecular beam epitaxy (MBE) equipped with a valved arsenic cracker source. The epitaxial structure is shown in Fig. 1(a). Prior to growth, the InP substrate was degassed at 400 °C in the preparation chamber of the MBE facility for 1 hour, followed by thermal deoxidation at 500 °C for 1 minute under As_2 overpressure protection. Then the n-type $In_{0.524}Al_{0.476}As$ and $In_{0.528}Al_{0.238}Ga_{0.234}As$ layers lattice-matched to InP were deposited at 500 °C and 485 °C, respectively. Si and Be were used as the n-type and p-type dopants, respectively. A 7-layer stacked QD structure was then deposited. For each QD layer, 6.8 monolayers (MLs) of InAs were directly grown on $In_{0.528}Al_{0.238}Ga_{0.234}As$ at 485 °C with a growth rate of 0.42 ML/s and an As_2/III ratio of 18, followed by a 10 second-growth interruption under As_2 pressure to stabilize QD formation and reduce island size dispersion. Then, the indium-flush technique was applied, where 2 nm $In_{0.359}Al_{0.323}Ga_{0.318}As$ stressor layer was deposited upon the dots, following a temperature elevation to 515 °C under As_2 overpressure with a beam equivalent pressure of 7×10^{-6} Torr for 3 minutes. The substrate was subsequently cooled to 485 °C to grow the 33 nm $In_{0.528}Al_{0.238}Ga_{0.234}As$ spacer layer. This indium-flush technique ensures the high-quality stacking of the QDs by manipulating the morphology and the strain around the QDs. Be-doped $In_{0.528}Al_{0.238}Ga_{0.234}As$ and $In_{0.524}Al_{0.476}As$ layers were then grown and covered by 10 nm Be-doped $In_{0.532}Ga_{0.468}As$, which served as a protection layer to alleviate oxidation during

Optics EXPRESS

transfer to metal-organic chemical vapor deposition (MOCVD) chamber. The doping density for n-type InAlAs was $5 \times 10^{18}\,cm^{-3}$ and the p-type InAlGaAs doping density was in the range of $5 \times 10^{16}\,cm^{-3}$ to $5 \times 10^{17}\,cm^{-3}$. 1700nm Zn-doped InP and 200 nm Zn-doped $In_{0.53}Ga_{0.47}As$ were then deposited in the MOCVD as cladding and p-type contact layers, respectively.

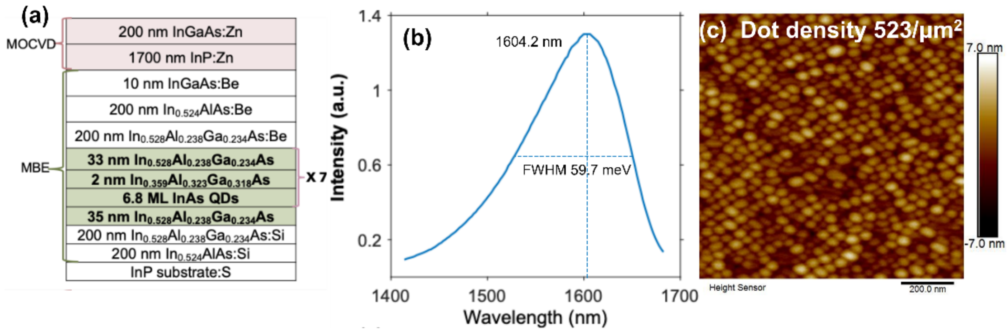

Fig. 1. (a) Schematic epitaxial structure of the InAs/InP QD laser. (b) RT PL spectrum of the seven-layer InAs/InP QD laser. (c) AFM image of uncapped InAs/InP QDs showing a high dot density of 523/μm^2.

The optical quality and morphology of the QDs were characterized separately using PL and atomic force microscope (AFM) measurements. As shown in Fig. 1(b), the 7-stack QD laser sample exhibits an L-band RT peak emission at 1604 nm with a narrow FWHM of 59.7 meV. Figure 1(c) shows a representative AFM image of the uncapped QDs with a scan area of 1×1 μm^2. The optimized combination of QD thickness, growth rate, substrate temperature and V/III ratio results in a uniform dot morphology and a high QD density of 523/μm^2.

The seven-stack InAs/InP QD Fabry-Pérot lasers were fabricated with a ridge width of 15 μm. The ridge waveguides were defined using conventional photolithography, followed by wet chemical etching and passivated with a 400 nm SiO_2 layer. A p-type metallization layer of Ti/Au (10/200 nm) was deposited on the exposed ridge top using a sputtering system, and the substrate was thinned to 150 μm. An n-type metallization of Ni/AuGe/Ni/Au (10/100/10/200 nm) was deposited on the backside of sample using a thermal evaporator. To form an Ohmic contact, the samples were annealed at 380 °C for 1 min. Laser bars were cleaved into different cavity lengths, ranging from 375 to 2000μm, without facet coatings. The fabricated lasers were characterized under pulsed injection (1% duty cycle, 1 μs pulse width) to minimize self-heating effects.

3. Results and discussion

Figure 2(a) shows the RT light-current (*L-I*) curves for InAs/InP QD lasers with cavity lengths ranging from 375 μm to 2000μm. The 2000 μm device exhibited the lowest J_{th} of 483 A/cm^2, corresponding to a J_{th} per QD layer of 69 A/cm^2. To the best of our knowledge, this is the lowest J_{th} per QD layer reported for C-/L-band InAs/InP QD lasers on (001) InP. Given that HR facet coatings are known to significantly reduce J_{th} [31], further optimization with HR coatings could achieve even lower J_{th}. The J_{th} for devices with cavity lengths of 1000, 750, 500, and 375 μm were measured to be 613, 833, 1189, and 1869 A/cm^2, respectively. Figure 2(b) illustrates J_{th} as a function of inverse cavity length, from which the transparency current density (J_{tr}) is extracted to be 130 A/cm^2, corresponding to a J_{tr} per QD layer of 18.6 A/cm^2.

In addition to the J_{th}, the temperature-insensitive operation is another crucial aspect of QD lasers. To evaluate the temperature-dependent performance across different cavity lengths (2000, 1000, and 500 μm), *L-I* measurements were performed over a wide temperature range. Figure 3(a) presents the temperature-dependent *L-I* curves under pulsed injection for a device with a cavity

Optics EXPRESS

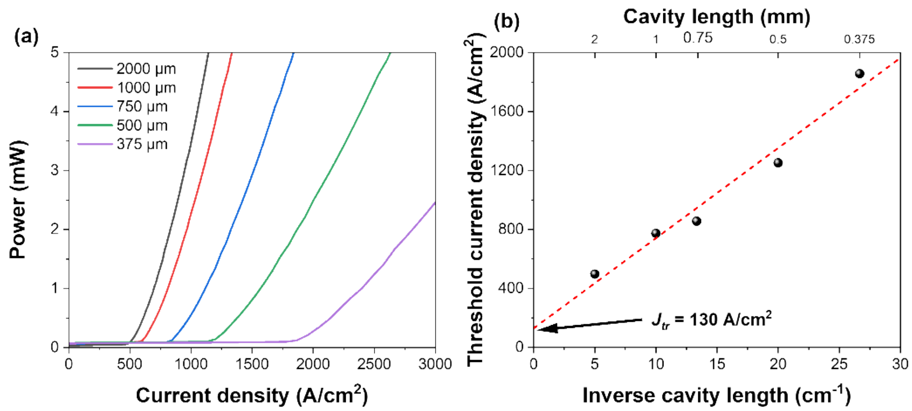

Fig. 2. (a) Power versus current density *L-I* curves under pulsed injection for InAs/InP QD lasers with a 15 µm cavity width and varied cavity lengths from 375 µm to 2000µm. (b) J_{th} as a function of the inverse cavity length for InAs/InP QD lasers.

length of 2000 µm. Note that the *L-I* curves for the 1000 and 500 µm devices are not shown here for brevity, as they exhibit similar trends. The maximum operating temperatures for devices with 2000, 1000, and 500 µm cavity lengths were 130, 120, and 120 °C, respectively. Notably, the device with 2000 µm cavity length achieved a maximum operating temperature of 130 °C, which is the highest operation temperature reported so far for an as-cleaved InAs/InP QD laser on (001) InP, although higher operation temperature was reported for HR-coated InAs/InP QD lasers [32]. Figure 3(b) shows the J_{th} as a function of temperature on a logarithmic scale. As expected, longer cavity devices exhibited lower J_{th} due to reduced mirror losses. The J_{th} maintained a nearly linear relationship over most of the temperature range, with slight deviations at 130 °C for the 2000 µm device. This deviation occurs at the maximum operating temperatures, indicating that thermal effects such as increased nonradiative recombination, thermally activated carrier leakage, and gain saturation become more significant near the device's operational limits. Additionally, at elevated temperatures, the thermal spreading of carriers among available states makes it more challenging to achieve the gain required to overcome losses, contributing to the observed rapid increase in J_{th} [33].

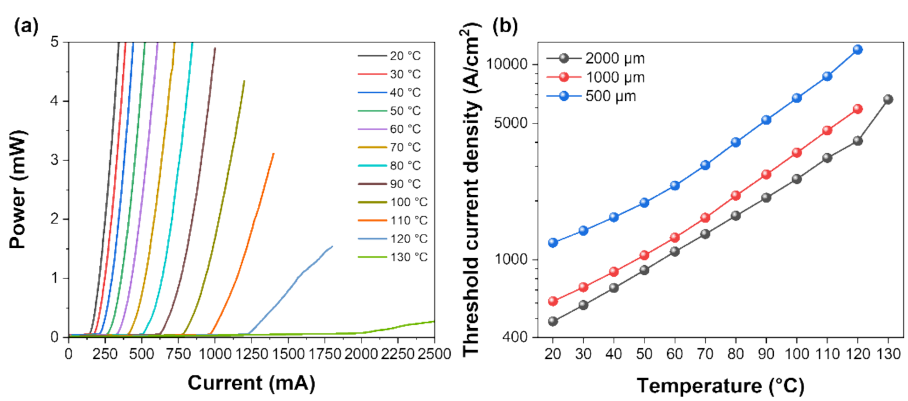

Fig. 3. (a) Temperature-dependent *L-I* characteristics of 2000 µm-long InAs/InP QD lasers under pulsed injection. (b) J_{th} versus temperature for InAs/InP QD lasers with cavity lengths of 2000, 1000, and 500 µm.

To quantitatively assess the temperature effects on the performance of QD lasers, the characteristic temperatures T_0 and T_1, which describe the temperature dependence of J_{th} and slope efficiency, respectively, were introduced. For the 2000, 1000, and 500 µm devices, the T_0 values were measured as 48.2 K, 50.9 K, 55.3 K below 70 °C, and 44.9 K, 39.0 K, and 37.2 K above 70 °C, respectively, as shown in Fig. 4(a). While the T_0 values remained relatively stable for the 2000 µm device across the temperature range, the 1000 µm and 500 µm devices exhibited more pronounced degradation at higher temperatures. This stronger degradation of T_0 with decreasing cavity length is mainly attributed to increased mirror losses, which lead to higher carrier densities and thus increased non-radiative recombination, as well as reduced heat dissipation [34]. In Fig. 4(b), the T_1 values for the 2000, 1000, and 500 µm devices were measured in two linear-fitted regions: 20–70 °C and 70–110 °C. The T_1 values for the 2000 µm device were 151.1 and 27.4 K for each respective region, while the 1000 and 500 µm devices exhibit T_1 values of 107.1 and 47.3 K, and 91.2, and 22.9 K, respectively. At lower temperatures (20–70 °C), longer cavity devices exhibit higher T_1 values due to lower mirror losses and reduced carrier leakage, leading to better slope efficiency retention. However, at higher temperatures (70–110 °C), the longest cavity (2000 µm) shows a noticeable degradation in T_1, indicating a pronounced decline in slope efficiency. This is predominantly driven by thermally activated carrier escape from QDs, which is more detrimental in longer cavity lengths due to their inherently lower carrier density [34]. As a result, longer cavities are generally more susceptible to the thermal carrier leakage at high temperatures, exacerbating slope efficiency degradation, compared to the shorter cavity length lasers. However, the device with the shortest cavity length of 500 µm exhibits the lowest T_1 value and more pronounced T_1 degradation than the 1000 um device at higher temperatures, which is consistent with other study [32]. This deviation in short cavity length is due to excessive mirror losses, which significantly increase carrier density and lead to enhanced non-radiative recombination. This mechanism becomes a major contributor to T_1 degradation in shorter cavities at high temperatures, contrasting with the thermal carrier escape that primarily affects longer cavities.

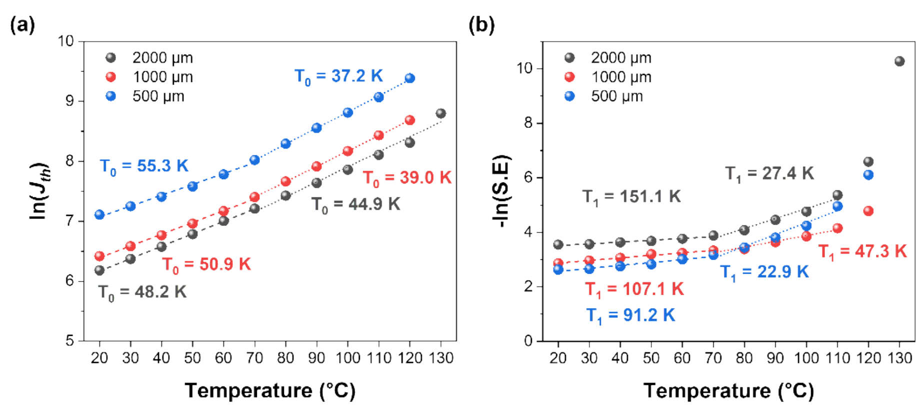

Fig. 4. Characteristic temperatures (a) T_0 and (b) T_1 for InAs/InP QD lasers with cavity lengths of 2000, 1000, and 500 µm.

The temperature-induced wavelength shift was also investigated. Figure 5(a) shows the RT peak lasing wavelengths for 2000, 1000, and 500 µm devices, measured to be 1624 nm, 1613 nm, and 1592 nm, respectively. The blue shift in shorter cavities is mainly driven by the increased threshold gain requirement due to higher mirror losses, which forces preferential lasing at shorter wavelengths where QD ensemble provides higher gain [35–37]. In addition, the interplay between larger mode spacing in shorter cavities and the asymmetric gain profile further restricts mode selection to the tail toward shorter wavelengths of the gain spectrum. Figure 5(b) presents the temperature-dependent peak lasing wavelength shifts for each device, measured at an injection current of 1.1 × threshold current (I_{th}). The 2000 and 1000 μm devices exhibited wavelength shifts of 0.37 nm/K and 0.35 nm/K, respectively. In contrast, the 500 μm device showed a relatively lower wavelength shift of 0.28 nm/K. The reduced wavelength shift rate in shorter cavity lengths is consistent with the results observed in other study on InAs/InP QD lasers [38]. The reduced temperature sensitivity in shorter cavities can be ascribed to two factors: (i) suppressed mode hopping due to larger longitudinal mode spacing, which relatively stabilizes the wavelength shift, leaving only the dominant intrinsic red-shifts from bandgap shrinkage and temperature-induced refractive index change, and (ii) enhanced contribution of smaller QDs and/or higher order transitions, driven by higher mirror losses that increase threshold gain requirement. Additional gain needed at elevated temperatures accelerates this effect as temperature increases, which forces the laser to favor lasing from smaller QDs (or higher energy transition) that inherently provide higher gain [36,38]. While all QDs undergo intrinsic redshift, the progressive inclusion of smaller QDs at higher temperatures introduces a partial blueshift, which offsets the intrinsic redshift.

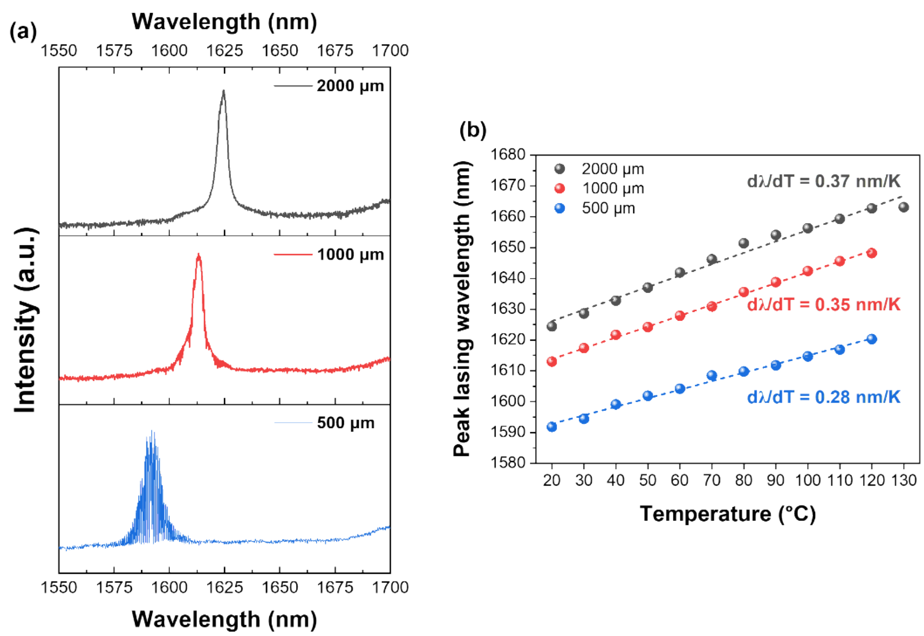

Fig. 5. (a) RT lasing spectra at an injection current of $1.1 \times I_{th}$ and (b) temperature-dependent peak lasing wavelengths of InAs/InP QD lasers with cavity lengths of 2000, 1000, and 500 μm.

It is noteworthy that further increasing the cavity length (e.g., 3000 μm) reduced the J_{th} further (440 A/cm^2, corresponding to 63 A/cm^2 per QD layer); however, such device exhibited a lower maximum operating temperature (110 °C) and evidence of mode hopping in the temperature-induced wavelength shift—namely, thermal and spectral instabilities. This observation suggests that an optimum cavity length exists where the trade-off between low J_{th} and high-temperature stability is balanced. In our study, the 2000 μm-long device is identified as an optimized cavity length, in terms of both J_{th} and temperature stability. For high-speed applications, such as directly modulated lasers, shorter cavity lengths may be preferable; however, additional measures—such as employing HR coatings to reduce mirror losses—would be necessary to maintain thermal stability. Additionally, we have achieved continuous-wave (CW) lasing with a RT J_{th} per QD layer of 187.1 A/cm^2 and a peak lasing wavelength shift of 0.76 nm/K in preliminary experiments, although the maximum operating temperature is currently limited to 35 °C for the 2000µm device. Further investigations—including the impact of cavity dimensions on thermal stability, detailed carrier transport modeling, and optimization of device processing—will be pursued in future work to enhance the CW performance.

4. Conclusion

In this study, low threshold L-band InAs/InAlGaAs/InP quantum dot (QD) lasers operating at high heat-sink temperatures were demonstrated. By applying an indium-flush technique, improved QD uniformity was achieved, leading to enhanced gain properties and temperature stability. The fabricated seven-stack as-cleaved lasers (15 µm × 2000µm) under pulsed injection exhibit a record-low threshold current density (J_{th}) of 69 A/cm^2 per QD layer, surpassing previously reported values for C-/L-band InAs/InP QD lasers on (001) InP, and a maximum operating temperature of 130 °C. In addition to these achievements, this study provides a comprehensive analysis of the effects of cavity length on temperature sensitivity and wavelength stability, offering valuable insights for optimizing InAs/InP QD lasers for specific applications. These results represent a significant step forward in the development of high-performance C-/L-band QD lasers in the InAs/InAlGaAs/InP material system, with potential applications in optical communication.

Funding. UK Engineering and Physical Sciences Research Council (EP/V029606/1, EP/V029681/1, EP/Z532848/1, EP/X015300/1, EP/T028475/1, EP/S024441/1, EP/P006973/1); European Union's Horizon 2020 program (101129904).

Disclosures. The authors declare no conflicts of interest.

Data availability. Data underlying the results presented in this paper are not publicly available at this time but may be obtained from the authors upon reasonable request.

References

1. M. Cantono, R. Schmogrow, M. Newland, *et al.*, "Opportunities and Challenges of C + L Transmission Systems," J. Lightwave Technol. **38**(5), 1050–1060 (2020).
2. T. Sakamoto, J. Kani, M. Jinno, *et al.*, "Wide wavelength band (1535–1560 nm and 1574–1600 nm), 28 × 10 Gbit/s WDM transmission over 320 km dispersion-shifted fibre," Electron. Lett. **34**(4), 392–394 (1998).
3. D. J. Klotzkin, *Introduction to Semiconductor Lasers for Optical Communications* (Springer International Publishing, 2020), Chap. 1.
4. P. Baziana, G. Drainakis, D. Georgantas, *et al.*, "AI and ML Applications Traffic: Designing Challenges for Performance Optimization of Optical Data Center Networks," in *International Conference on Software, Telecommunications and Computer Networks* (2024), pp. 1–6.
5. Y. Arakawa and H. Sakaki, "Multidimensional quantum well laser and temperature dependence of its threshold current," Appl. Phys. Lett. **40**(11), 939–941 (1982).
6. K. Nishi, K. Takemasa, M. Sugawara, *et al.*, "Development of Quantum Dot Lasers for Data-Com and Silicon Photonics Applications," IEEE J. Sel. Top. Quantum Electron. **23**(6), 1–7 (2017).
7. H. Y. Liu, I. R. Sellers, T. J. Badcock, *et al.*, "Improved performance of 1.3µm multilayer InAs quantum-dot lasers using a high-growth-temperature GaAs spacer layer," Appl. Phys. Lett. **85**(5), 704–706 (2004).
8. J. Duan, H. Huang, B. Dong, *et al.*, "1.3- µm Reflection Insensitive InAs/GaAs Quantum Dot Lasers Directly Grown on Silicon," IEEE Photonics Technol. Lett. **31**(5), 345–348 (2019).
9. T. W. Berg, S. Bischoff, I. Magnusdottir, *et al.*, "Ultrafast gain recovery and modulation limitations in self-assembled quantum-dot devices," IEEE Photonics Technol. Lett. **13**(6), 541–543 (2001).
10. S. Chen, W. Li, J. Wu, *et al.*, "Electrically pumped continuous-wave III–V quantum dot lasers on silicon," Nat. Photonics **10**(5), 307–311 (2016).
11. Y. Wang, S. Chen, Y. Yu, *et al.*, "Monolithic quantum-dot distributed feedback laser array on silicon," Optica **5**(5), 528–533 (2018).
12. S. Liu, X. Wu, D. Jung, *et al.*, "High-channel-count 20 GHz passively mode-locked quantum dot laser directly grown on Si with 4.1 Tbit/s transmission capacity," Optica **6**(2), 128–134 (2019).
13. W.-Q. Wei, A. He, B. Yang, *et al.*, "Monolithic integration of embedded III-V lasers on SOI," Light: Sci. Appl. **12**(1), 84 (2023).
14. Q. Feng, W. Wei, B. Zhang, *et al.*, "O-Band and C/L-Band III-V Quantum Dot Lasers Monolithically Grown on Ge and Si Substrate," Appl. Sci. **9**(3), 385 (2019).
15. M. L. Osowski, Y. Gewirtz, R. M. Lammert, *et al.*, "High-power semiconductor lasers at eye-safe wavelengths," in *Laser Technology for Defense and Security V* (SPIE, 2009), 7325, pp. 184–190.

Optics EXPRESS

16. S. Bauer, V. Sichkovskyi, O. Eyal, *et al.*, "1.5-μm Indium Phosphide-Based Quantum Dot Lasers and Optical Amplifiers: The Impact of Atom-Like Optical Gain Material for Optoelectronics Devices," IEEE Nanotechnol. Mag. **15**(2), 23–36 (2021).
17. Z. G. Lu, J. R. Liu, S. Raymond, *et al.*, "312-fs pulse generation from a passive C-band InAs/InP quantum dot mode-locked laser," Opt. Express **16**(14), 10835–10840 (2008).
18. D. Gready, G. Eisenstein, V. Ivanov, *et al.*, "High Speed 1.55 μm InAs/InGaAlAs/InP Quantum Dot Lasers," IEEE Photonics Technol. Lett. **26**(1), 11–13 (2014).
19. A. Becker, V. Sichkovskyi, M. Bjelica, *et al.*, "Narrow-linewidth 1.5-um quantum dot distributed feedback lasers," in Novel In-Plane Semiconductor Lasers XV (2016), 9767, pp. 99–106.
20. J. Kwoen, N. Morais, W. Zhan, *et al.*, "All III-arsenide low threshold InAs quantum dot lasers on InP(001)," Electron. Lett. **59**(16), e12920 (2023).
21. P. Caroff, C. Paranthoen, C. Platz, *et al.*, "High-gain and low-threshold InAs quantum-dot lasers on InP," Appl. Phys. Lett. **87**(24), 243107 (2005).
22. S. G. Li, Q. Gong, C. F. Cao, *et al.*, "The developments of InP-based quantum dot lasers," Infrared Phys. Technol. **60**, 216–224 (2013).
23. A. Ponchet, L. Pedesseau, A. Le Corre, *et al.*, "Shape transition in InAs nanostructures formed by Stranski-Krastanow growth mode on InP (001) substrate," Appl. Phys. Lett. **114**(17), 173102 (2019).
24. S. Yoon, Y. Moon, T.-W. Lee, *et al.*, "Effects of As/P exchange reaction on the formation of InAs/InP quantum dots," Appl. Phys. Lett. **74**(14), 2029–2031 (1999).
25. S. Bauer, V. Sichkovskyi, and J. P. Reithmaier, "Growth and optical characteristics of InAs quantum dot structures with tunnel injection quantum wells for 1.55 μm high-speed lasers," J. Cryst. Growth **491**, 20–25 (2018).
26. M. Z. M. Khan, T. K. Ng, and B. S. Ooi, "Self-assembled InAs/InP quantum dots and quantum dashes: Material structures and devices," Prog. Quantum Electron. **38**(6), 237–313 (2014).
27. J. F. Girard, C. Dion, P. Desjardins, *et al.*, "Tuning of the electronic properties of self-assembled InAs/InP(001) quantum dots by rapid thermal annealing," Appl. Phys. Lett. **84**(17), 3382–3384 (2004).
28. B. Shi and K. M. Lau, "Enhanced optical properties of InAs/InAlGaAs/InP quantum dots grown by metal-organic chemical vapor deposition using a double-cap technique," J. Cryst. Growth **433**, 19–23 (2016).
29. J. Yuan, C. Dear, H. Jia, *et al.*, "Indium-flush technique for C-band InAs/InP quantum dots," APL Mat. **12**(12), 121109 (2024).
30. B. Wang, X. Yu, Y. Zeng, *et al.*, "InAs quantum dots with a narrow photoluminescence linewidth for a lower threshold current density in 1.55 μm lasers," Opt. Mater. Express **14**(4), 1074–1084 (2024).
31. H. Saito, K. Nishi, and S. Sugou, "Ground-state lasing at room temperature in long-wavelength InAs quantum-dot lasers on InP(311)B substrates," Appl. Phys. Lett. **78**(3), 267–269 (2001).
32. A. Abdollahinia, S. Banyoudeh, A. Rippien, *et al.*, "Temperature stability of static and dynamic properties of 1.55 μm quantum dot lasers," Opt. Express **26**(5), 6056–6066 (2018).
33. P. M. Smowton, S. N. Elliott, S. Shutts, *et al.*, "Temperature-Dependent Threshold Current in InP Quantum-Dot Lasers," IEEE J. Sel. Top. Quantum Electron. **17**(5), 1343–1348 (2011).
34. L. A. Coldren, S. W. Corzine, and M. L. Mashanovitch, *Diode Lasers and Photonic Integrated Circuits* (John Wiley & Sons, 2012), Chap. 2.
35. J. Z. Wilcox, S. Ou, J. J. Yang, *et al.*, "Dependence of emission wavelength on cavity length and facet reflectivities in multiple quantum well semiconductor lasers," Appl. Phys. Lett. **54**(22), 2174–2176 (1989).
36. F. Klopf, S. Deubert, J. P. Reithmaier, *et al.*, "Correlation between the gain profile and the temperature-induced shift in wavelength of quantum-dot lasers," Appl. Phys. Lett. **81**(2), 217–219 (2002).
37. R. Debusmann, T. W. Schlereth, S. Gerhard, *et al.*, "Gain studies on quantum-dot lasers with temperature-stable emission wavelength," IEEE. J. Quantum Electron. **44**(2), 175–181 (2008).
38. V. I. Sichkovskyi, M. Waniczek, and J. P. Reithmaier, "High-gain wavelength-stabilized 1.55 μm InAs/InP(100) based lasers with reduced number of quantum dot active layers," Appl. Phys. Lett. **102**(22), 221117 (2013).